the test animal to remain on a rotating rod (rotorod test).[28] In addition, spontaneous locomotor activity of mice was measured by an automated procedure.[29] Rats were tested for drug-induced alterations of electrical self-stimulation of the brain (methods of ref 26a). Rats were tested against maximal electroshock (methods of ref 25) and in a subjective assessment of behavioral impairment. Median effective doses were determined by a probit analysis.[30]

Acknowledgment. We thank Dr. F. A. MacKellar and his associates for IR and NMR spectra as well as for the elemental analyses and M. Vartanian, P. Mickevicius, and B. Stieber (Warner-Lambert) for pharmacological test results. The help of the Antiepileptic Drug Development Program, Epilepsy Branch, NINCDS (H. J. Kupferberg and G. Gladding), in the pharmacological evaluation of several of these compounds is gratefully acknowledged.

Registry No. 1 des-1-oxide, 2176-45-6; 1·H_2SO_4 (des-1-oxide), 65846-21-1; **2**, 32967-12-7; **3**, 81911-41-3; **3**·HCl, 112945-84-3; **3** des-1-oxide, 54629-96-8; **4**, 112945-85-4; **4** des-1-oxide, 75580-04-0; **5**, 112945-86-5; **6**, 112945-87-6; **6** des-1-oxide, 76167-46-9; **7**, 112946-02-8; **7**·HCl, 112945-88-7; **7** des-1-oxide, 73406-90-3; **8**, 112945-89-8; **8** des-1-oxide, 78790-74-6; **9**, 112945-90-1; **9** des-1-oxide, 28232-56-6; **10**, 112946-03-9; **10**-HCl, 112945-91-2; **10** des-1-oxide, 112968-85-1; **11**, 112946-04-0; **11**-HCl, 112945-92-3; **11** des-1-oxide, 28232-60-2; **12**, 112946-05-1; **12**-CHCl, 112945-93-4; **13**, 112945-94-5; **14**, 112945-95-6; **15**, 112945-96-7; **15** des-1-oxide, 54629-99-1; **16**, 112945-97-8; **16** des-1-oxide, 112946-08-4; **17**, 112945-98-9; **17** des-1-oxide, 112946-09-5; **18**, 112945-99-0; **18** des-1-oxide, 112946-10-8; **19**, 112946-00-6; **19** des-1-oxide, 112946-11-9; **20**, 112946-01-7; **21**, 38674-06-5; **22**, 54629-29-7; isonicotinic acid, 55-22-1; 2-chloro-3-phenoxypyridine, 73406-93-6; 4-((hydroxyimino)methyl)-3-phenoxypyridine, 112946-06-2; (3-phenoxy-4-pyridyl)methyl acetate, 112946-07-3; 5-methyl-3-phenoxypyridine, 73571-20-7; 4-(trifluoromethyl)pyridine, 3796-24-5.

(27) Coughenour, L.; McLean, J. R.; Parker, R. *Pharmacol. Biochem. Behav.* **1977**, *6*, 351.
(28) Dunham, N. W.; Miya, T. A. *J. Am. Pharm. Assoc., Sci. Ed.* **1957**, *46*, 208.
(29) McLean, J. R.; Parker, R.; Coughenour, L. *Life. Sci.* **1978**, *22*, 1067.
(30) Litchfield, J. T.; Wilcoxon, F. *J. Pharmacol.* **1949**, *96*, 99.

Synthesis, Molecular Modeling, DNA Binding, and Antitumor Properties of Some Substituted Amidoanthraquinones

David A. Collier and Stephen Neidle*

Cancer Research Campaign Biomolecular Structure Unit, The Institute of Cancer Research, Sutton, Surrey, SM2 5PX U.K.
Received April 30, 1987

A series of 1- and 1,4-substituted amidoanthraquinones have been prepared, with side chains possessing basic nitrogen atoms. Computer modeling and energy calculations have shown that all eight compounds can bind intercalatively to DNA and that there are significant differences in the additional nonbonded and electrostatic interactions possible at the DNA binding site. Solution DNA binding and closed-circular DNA unwinding studies confirmed intercalative interactions, and the predicted differences in strength of interactions between mono- and disubstituted compounds were found. All compounds were modestly cytotoxic to L1210 cells in culture. In vivo activity against L1210 and S180 tumors was not found for the monosubstituted compounds, whereas the four disubstituted ones had varying levels of measurable, though low, activity.

The clinical utility of the anthracycline antitumor antibiotics, especially the broad spectrum activity of Adriamycin, is hampered by their severe dose-limiting, cumulative cardiotoxicity.[1] There has accordingly been a continuing search for analogues with diminished toxicity, as well as with improved therapeutic indices.[2] An area of particular activity and promise is concerned with aminoalkyl-substituted anthraquinones[3-6] with the demonstration of clinical activity for the 1,4-disubstituted compound mitoxantrone (1).[7,8] Although the precise mode of action in vivo for these compounds has not been fully elucidated, a number of studies have shown that they interact intercalatively with DNA in vitro[9-15] and that therefore DNA is a major biological target for mitoxantrone.

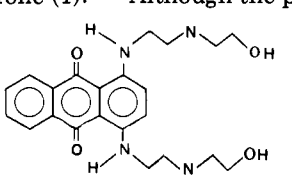

1

The present study examines the DNA-interactive abilities, both calculated the experimental, of a new series of 1-mono- and 1,4-disubstituted alkylamido-substituted anthraquinones.[1-8] These are examined in relation to their cytotoxic and antitumor properties. Earlier studies by Palumbo et al. have shown direct relationships between DNA-binding parameters and at least some biological

(1) Hoffman, D. H.; Benjamin, R. S.; Bachur, N. R. *Clin. Pharmacol. Ther. (St. Louis)* **1972**, *13*, 895.
(2) Arcamone, F. *Antitumor Antibiotics*; Academic: New York, 1981.
(3) Murcock, K. C.; Child, R. C.; Fabio, P. F.; Angier, R. B.; Wallace, R. E.; Durr, F. E.; Citarella, R. V. *J. Med. Chem.* **1979**, *22*, 1024.
(4) Zee-Cheng, R. K.-Y.; Cheng, C. C. *J. Med. Chem.* **1978**, *21*, 291.
(5) Cheng, C. C.; Zee-Cheng, R. K.-Y. *Prog. Med. Chem.* **1983**, *20*, 83.
(6) Krapcho, A. P.; Landi, J. J.; Shaw, K. J.; Phinney, D. G.; Hacker, M. P.; McCormack, J. J. *J. Med. Chem.* **1986**, *29*, 1370.
(7) Stuart-Harris, R. C.; Smith, I. E.; *Cancer Chemother. Pharmacol.* **1982**, *8*, 179.
(8) Estey, E. H.; Keating, M. J.; McCredie, K. B.; Bodey, G. P.; Freireich, E. J. *Cancer Treat. Rep.* **1983**, *67*, 389.
(9) Foye, W. D.; Vajrargupta, O.; Sengupta, S. K. *J. Pharm. Sci.* **1982**, *71*, 253.
(10) Kapuscinski, J.; Darzynkiewicz, Z.; Traganos, F.; Melamed, M. R. *Biochem. Pharmacol.* **1981**, *30*, 231.
(11) Lown, J. W.; Hanstock, C. C.; Bradley, R. D.; Scraba, D. G. *Mol. Pharmacol.* **1984**, *25*, 178.
(12) Islam, S. A.; Neidle, S.; Gandecha, B. M.; Partridge, M.; Patterson, L. H.; Brown, J. R. *J. Med. Chem.* **1985**, *28*, 857.
(13) Kotovych, G.; Lown, J. W.; Tong, J. P. K. *J. Biomol. Struct. Dyn.* **1986**, *4*, 111.
(14) Lown, J. W.; Morgan, A. R.; Yen, S.-F.; Wang, Y.-H.; Wilson, W. D. *Biochemistry* **1985**, *24*, 4028.
(15) Krishnamoorthy, C. R.; Yen, S.-F.; Smith, J. C.; Lown, J. W.; Wilson, W. D. *Biochemistry* **1986**, *25*, 5933.

0022-2623/88/1831-0847$01.50/0

Table I. ΔT_m Values for Compounds **2–9**

drug	ΔT_m calf thymus DNA	ΔT_m poly[d(A)]·poly[d(T)]	ΔT_m poly[d(AT)]·poly[d(AT)]
2	9.0	1.5	12.0
3	9.0	3.0	12.4
4	10.5	2.5	12.5
5	8.5	2.0	13.0
6		9.0[a]	28.0[a]
7		8.0[a]	29.2[a]
8		8.0[a]	30.5[a]
9		7.0[a]	27.0[a]

[a] Bisphasic melting curves were recorded.

effects for a series of monosubstituted amidoanthraquinones.[16-18] In the present paper, we also report on molecular-modeling studies of interactions between the (alkylamido)anthraquinones and models for DNA. We have previously shown[12] that these can provide information relevant both to DNA interaction in solution and to relative cytotoxicities within a series.

Results

Chemistry. Compounds **2–9** were all synthesized by a two-stage reaction. The first stage involves the reaction of an appropriate acid chloride with an amino-substituted anthraquinone, in an inert and dry solvent,[19,20] with a catalytic quantity of pyridine, producing the mono- and disubstituted compounds **10** and **11**. These chloropropanamides were coupled to secondary amines to give the alkylamino derivatives **2–9** (in high yield) with the elimination of HCl. No attempt was made to separate the stereoisomers of **9**, which has two asymmetric centers.

DNA Binding in Solution. Several techniques were used to study the DNA-interactive properties of compounds **2–9**. The extent to which ligands stabilize the helix coil thermal transition of double-stranded DNA can be taken as an overall indication of the strength and extent of binding,[21] although not of the mode of interaction. The results of the melting-curve studies (Table I) show that all of the compounds produce positive T_m increases in nucleic acid melting temperatures; compounds 6–9 stabilized calf thymus DNA at the phosphate:drug ratio used (10:1) to such an extent that it did not fully melt below 99 °C. Similar effects were found with GC-containing synthetic polynucleotides. Compounds **2–5** showed minimal stabilization of the synthetic polymer poly[d(A)]·poly[d(T)], in contrast to the much higher levels shown with the alternating polymer poly[d(AT)]·poly[d(AT)]. Compounds **6–9** consistently gave much higher T_m values (and biphasic melting curves) compared to their monosubstituted counterparts **2–5**. Mitoxantrone gave a T_m of 15.9 °C with calf thymus DNA under the conditions used.

Equilibrium binding constants for the interactions of compounds **2–9** with calf thymus DNA are obtained by spectrophotometric analysis.[22] Scatchard plots obtained were nonlinear, indicating neighbor-exclusion and/or heterogeneity of binding sites.[23] The binding isotherms were fitted to the nonlinear McGhee–Von Hippel model,[24] and values for the equilibrium constant $K(0)$ and number of base pairs per binding site, were obtained (Table II). Kinetic effects related to addition of DNA were not observed, and it was therefore assumed that equilibrium between free and bound drug species was quickly reached.

The effect of compounds **2–9** on the superhelicity of covalently closed circular DNA was studied by monitoring the viscosity changes produced upon drug binding.[25-27] All the compounds unwound and reversed the superhelicity

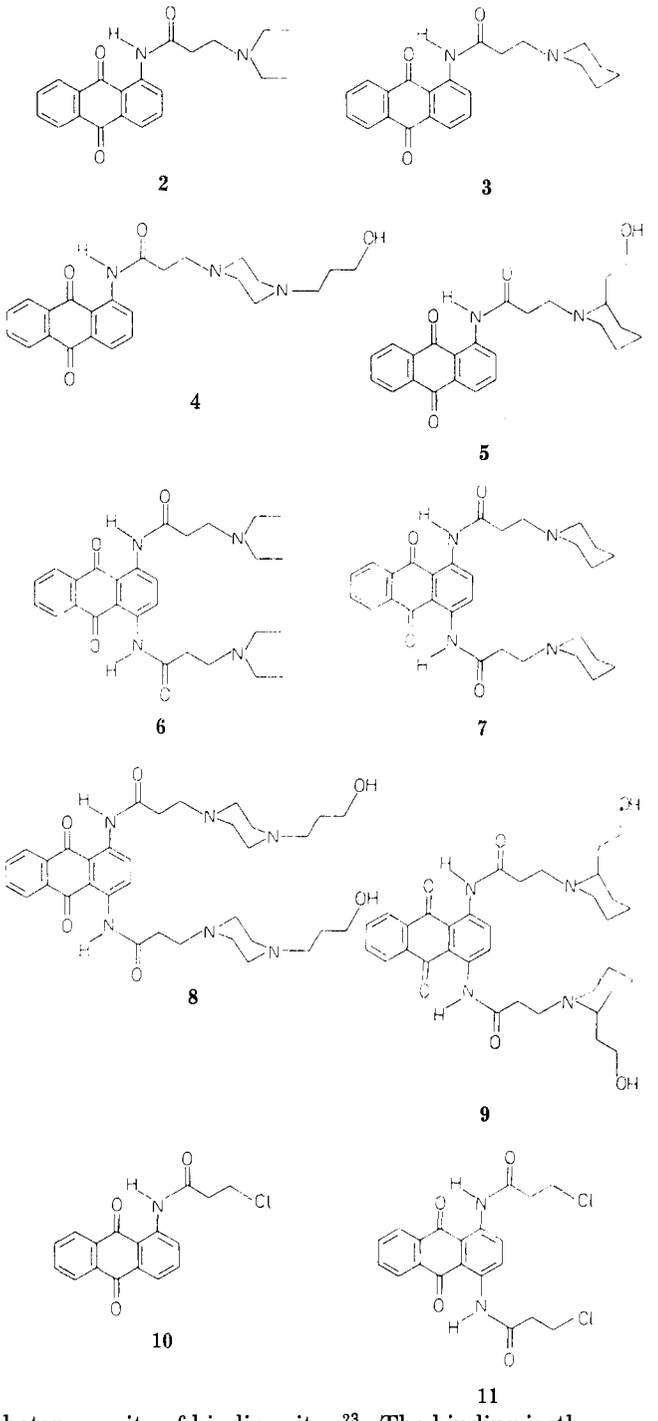

(16) Palumbo, M.; Magno, S. M. *Int. J. Biol. Macromol.* **1983**, *5*, 301.
(17) Palumbo, M.; Antonello, C.; Viano, I.; Santiano, M.; Gia, O.; Gastaldi, S.; Magno, S. M. *Chem.-Biol. Interact.* **1983**, *44*, 207.
(18) Palii, G.; Palumbo, M.; Antonello, C.; Meloni, G. A.; Magno, S. M. *Mol. Pharmacol.* **1986**, *29*, 211.
(19) Marschalk, C. *Bull. Soc. Chim. Fr.* **1952**, *19*, 955.
(20) Hromatka, O.; Knollmuller, M.; Maier, K.; Gotschy, F. *Monatsch. Chem.* **1969**, *100*, 1391.
(21) Crothers, D. M. *Biopolymers* **1971**, *10*, 2147.
(22) Peacocke, A. R.; Skerrett, J. N. H. *Trans. Faraday Soc.* **1956**, *52*, 261.
(23) Dougherty, G.; Pigram, W. J. *CRC Crit. Rev. Biochem.* **1982**, *12*, 103.
(24) McGhee, J. D.; Von Hippel, P. H. *J. Mol. Biol.* **1974**, *86*, 469.
(25) Crawford, L. V.; Waring, M. J. *J. Mol. Bio.* **1967**, *25*, 23.
(26) Bauer, W.; Vinograd, J. *J. Mol. Biol.* **1968**, *33*, 141.
(27) Revet, B. M. J.; Schmir, M.; Vinograd, J. *Nature (London), New Biol.* **1971**, *229*, 10.

Table II. DNA Binding Parameters for Compounds **2–9**

drug	free		fully bound		isosbestic point, nm	n	$K(0)$, $M^{-1} \times 10^5$
	ϵ	λ_{max}, nm	ϵ	λ_{max}, nm			
2	4557	396.0	4212	411	417	4.2	1.6
3	4489	397.0	4150	411	418	4.3	1.6
4	4369	397.5	4045	411	418	3.9	1.8
5	4582	395.0	4241	410	416	4.1	1.7
6	4963	447.0	4447	461	465	5.5	2.4
7	5691	445.0	5133	460	464	5.1	2.2
8	5477	447.0	4963	461	484	5.0	2.9
9	5273	447.5	4724	460	464	5.3	2.5

Table III. Unwinding Angles for Compounds **2–9**

drug	unwinding angle (±0.3)	drug	unwinding angle (±0.3)
2	15.5	**6**	15.6
3	15.5	**7**	16.3
4	15.9	**8**	16.1
5	15.6	**9**	15.8

of supercoiled plasmid DNA, with behavior analogous to that found for other DNA-binding ligands of known intercalative behavior (for example, in ref 28). The calculated unwinding angles, in Table III, are relative to a value of 26° for ethidium.[29]

Crystallography. The molecular structure of a representative amidoanthraquinone (**4**) in the series was determined by X-ray crystallography in order to obtain geometric and conformational information needed for subsequent computer modeling. A view of the structure is shown in Figure 1. The amide group is coplanar with the anthraquinone ring, and there is an intramolecular hydrogen bond between the amide hydrogen atom and the quinoid oxygen atom on the ring (HN1···O9 distance of 1.84 Å). The amide group itself has a trans conformation, with an amide torsion angle of 178°. The piperazine ring and its hydroxylpropyl substituent are arranged in an elongated manner with respect to the anthraquinone ring, so that the molecule as a whole has an L-shape.

Molecular Modeling. Computerized molecular modeling and approximate energy calculations were used to visualize and estimate potential complexes between compounds **2–9** and double-stranded DNA. Since the DNA-binding data in solution for these compounds indicates that intercalation is their primary mode of noncovalent binding (see below), a model for intercalation was used that was based on the crystal structure of a proflavine–deoxydinucleoside duplex complex.[12,20-32] Both AT and GC sites were examined with a view to establishing plausible geometries and patterns of potential hydrogen bonding between drug and receptor binding site. During the interactive graphics modeling process, the conformations of drug side chains were altered so as to form and optimize potential attractive nonbonded contacts, as well as to minimize repulsive ones. Energies were calculated by use of a semiempirical force field that previous studies[31] have found to satisfactorily rank possible intercalation geometries in energetic terms that accord well with experimental binding affinities. It must be emphasized that this approach is not designed to provide exact quantitations of intermolecular and intramolecular energies; this would not have been possible for the large number of compounds and binding modes examined, not least in view of the very large amount of computational resource that would be needed. Thus, the energetic terms presented here are to be taken only as a guide to relative differences and ranking orders of site affinities.

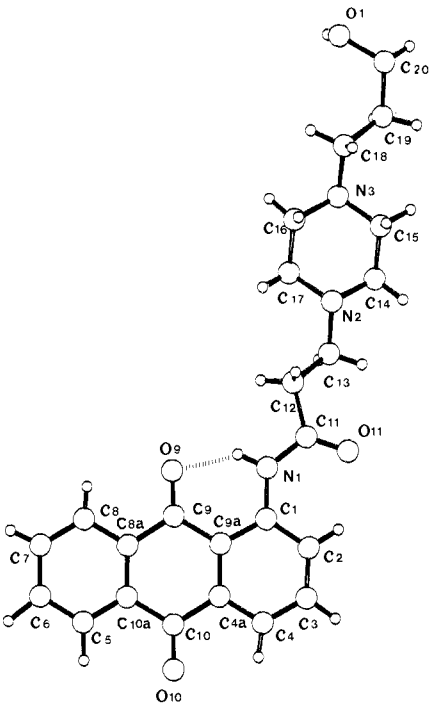

Figure 1. A computer-drawn plot of the molecular structure of compound **4** as a free base, determined by X-ray crystallographic analysis. The dashed line indicates an intramolecular hydrogen bond.

Geometries for **2** and **5–9** (as protonated species) were derived from that of the experimentally determined structure of **4** by using standard geometric considerations. Detailed modeling was not performed on compound **3** as preliminary results indicated no significant differences compared to **2**. Tables V and VI detail energetic and hydrogen-bonding parameters for interactions between **2–9** and the d(CpG) duplex, and Figures 2–4 illustrate several of these low-energy states. For compounds **2–5**, intercalation can occur with the single side chain in either the wide major or the narrower minor groove. The major groove is suggested to be preferred for the side chains, on account of the more favorable electrostatic interactions between phosphate groups of the dinucleoside backbone and side-chain protonated amino groups of the drugs; however, since the energy calculations were limited in extent and did not consider solvent, we cannot be firm on this point. Compound **4** was able to form stereochemically acceptable hydrogen bonds between the terminal hydroxyl

(28) Kitchen, S. E.; Wang, J.-H.; Baunstark, A. L.; Wilson, W. D.; Boykin, D. W. *J. Med. Chem.* **1985**, *28*, 940.
(29) Wang, J. C. *J. Mol. Biol.* **1974**, *89*, 783.
(30) Shieh, H.-S.; Berman, H. M.; Dabrow, M.; Neidle, S.; *Nucleic Acids Res.* **1980**, *8*, 85.
(31) Islam, S. A.; Neidle, S. *Acta Crystallogr., Sect. B: Struct. Sci.* **1984**, *B40*, 424.
(32) Neidle, S.; Webster, G. D.; Baguley, B. C.; Denny, W. A. *Biochem. Pharmacol.* **1986**, *35*, 3915.

Table IV. Atomic Coordinates for 4, with Estimated Standard Deviations in Parentheses[a]

atom	x	y	z	B, Å^2
O1	1.0584 (2)	0.2974 (4)	−0.0743 (1)	4.53 (6)
O9	0.8828 (1)	0.1310 (4)	0.4662 (1)	4.48 (6)
O10	0.6812 (2)	0.1249 (6)	0.6251 (1)	7.21 (9)
O11	0.6295 (2)	0.1752 (6)	0.2526 (1)	7.41 (9)
N1	0.7384 (2)	0.1465 (4)	0.3566 (1)	3.38 (6)
N2	0.8039 (2)	0.2358 (4)	0.1490 (1)	3.12 (6)
N3	0.9004 (2)	0.3098 (4)	0.0569 (1)	3.05 (6)
C1	0.6886 (2)	0.1401 (5)	0.3995 (1)	2.79 (7)
C2	0.5933 (2)	0.1388 (6)	0.3742 (2)	3.65 (8)
C3	0.5465 (2)	0.1345 (6)	0.4173 (2)	3.86 (9)
C4	0.5896 (2)	0.1339 (6)	0.4866 (2)	3.78 (8)
C4A	0.6837 (2)	0.1327 (5)	0.5138 (2)	3.04 (7)
C5	0.8690 (2)	0.1546 (6)	0.6886 (2)	4.49 (9)
C6	0.9621 (3)	0.1650 (7)	0.7157 (2)	5.1 (1)
C7	1.0130 (2)	0.1598 (6)	0.6745 (2)	4.6 (1)
C8	0.9714 (2)	0.1146 (6)	0.6050 (2)	3.85 (9)
C8A	0.8775 (2)	0.1384 (5)	0.5761 (2)	2.92 (7)
C9A	0.7345 (2)	0.1349 (5)	0.4705 (1)	2.53 (7)
C9	0.8350 (2)	0.1342 (5)	0.5010 (1)	2.93 (7)
C10	0.7265 (2)	0.1328 (6)	0.5887 (2)	4.04 (9)
C10A	0.8269 (2)	0.1426 (5)	0.6183 (2)	3.32 (8)
C11	0.7083 (2)	0.1659 (6)	0.2877 (2)	4.21 (9)
C12	0.7830 (2)	0.1693 (7)	0.2583 (2)	4.9 (1)
C13	0.7569 (2)	0.2908 (6)	0.1945 (2)	4.45 (9)
C14	0.8994 (2)	0.2943 (6)	0.1736 (2)	3.85 (9)
C15	0.9444 (2)	0.2261 (6)	0.1250 (2)	3.66 (8)
C16	0.8041 (2)	0.2600 (5)	0.0332 (2)	3.35 (8)
C17	0.7605 (2)	0.3258 (6)	0.0823 (2)	3.48 (8)
C18	0.9416 (2)	0.2317 (6)	0.0094 (2)	3.70 (8)
C19	0.9114 (2)	0.3370 (6)	−0.0581 (2)	3.91 (9)
C20	0.9620 (2)	0.2763 (6)	−0.1040 (2)	4.5 (1)

[a] The thermal parameters are the averaged B_{ii} values for each anisotropically refined atom.

Table V. Binding of Compounds 2–9 to a Deoxycytidyl-(5′→3′)-deoxyguanosine (d(CpG)) Fragment as Modeled by Computer Graphics

compd	binding mode	energy, kcal mol^{-1} E_{TOT}	energy, kcal mol^{-1} E_{E-S}	no. of hydrogen bonds
2′	minor groove	−63.7	−11.1	0
2″	major groove	−67.1	−11.1	1
4′	minor groove	−70.0	−9.7	0
4″	major groove	−86.9	−31.0	2
5′	minor groove	−73.0	−7.5	3
5″	major groove	−75.3	−17.8	2
6′	major groove	−95.8	−28.8	2
6″	spear mode	−84.4	−13.4	1
8′	major groove	−130.5	−61.5	4
8″	spear mode	−113.9	−43.6	3
9′	major groove	−108.6	−28.0	4
9″	spear mode	−95.9	−27.9	2

group on its side chain and guanine base atoms N2 and N3. Parallel modeling studies with the duplex of d(TpA) produced overall similar results (Table VII), although the details of intermolecular interactions were in some cases distinct.

The disubstituted amidoanthraquinones **6–9** produced low-energy intercalated geometries with the side chains lying either in the major groove, or alternatively in a spear mode,[12,33] with one side chain and its substituents in each groove (Figure 3). With the spear mode in the latter mode, interactions involved major groove phosphates. In the minor groove, the drug side chains were not of sufficient length to contact them. These 1,4 compounds were found to be excluded from having both side chains in the minor groove on account of steric hindrance with the sugar–phosphate backbones. The Y-shape of these molecules imposed by the rigid amide group imposes on them a width greater than that of the narrow minor groove. The majority of nonbonded interactions between drug and DNA for **6–9** involved phosphate groups and side-chain substituent cationic nitrogen atoms. Only in the case of **9** was it possible to form satisfactory hydrogen bonds with base atoms (N7 of guanine) such that in the major groove a symmetrical arrangement involved N7 of both strands. Compound **8** was able to produce the energetically most stable complexes, for both d(CpG) and d(TpA) sequences, on account of the greater number of ionic interactions possible with this compound. In general, the disubstituted amidoanthraquinones were computed to have a greater interaction energy with the model DNA intercalation sites than their monocounterparts, in large part because of the greater number of potential ionic-type interactions.

Tumor Model Systems. The cytotoxic effects in cell culture of compounds **2–9** were evaluated in comparison with mitoxantrone with use of a L1210 cell line. The results of this study, in Table VIII, show that the disubstituted compounds **6–9** in the series have inhibitory effects on cell growth 1 order of magnitude greater than those of their monosubstituted counterparts, and that compounds **6**, **7**, and **9** approach mitoxantrone in their effects. The two compounds with (hydroxypropanyl)piperazine substituents (**4** and **8**) have notably greater cytotoxicities than others in the group. In vivo effects were evaluated against L1210 and S180 (murine) tumor models. Compounds **2–5** showed no significant activity in the L1210 leukemia model, when dosed once daily. Compounds **6–9** showed moderate activity, giving percentage increases in life span of 21–36% at the optimum dosage level used, 12.5 mg kg^{-1}, depending on the compound (Table X). Double this dosage level produced a fall-off in activity, presumably as a result of increased toxicity. In an attempt to ameliorate toxicity and increase activity, the compounds were dosed twice daily at 12.5 mg kg^{-1}. Percentage increases in life

(33) Collier, D. A.; Neidle, S.; Brown, J. R. *Biochem. Pharmacol.* 1984, *33*, 2877.

Table VI. Geometry of and Atoms Involved in Hydrogen Bonding with the d(CpG) Fragment[a]

compound	atoms			distances		angle, deg
	1	2	3	2–3	1–3	
2′						
2″	N2	HN2	O1A	1.94	2.91	163
3′						
3″	N2	HN2	O1A	2.07	3.06	170
	N3	NH3	O1A	1.99	2.99	173
5′	O2	HO2	N2G1	2.50	3.12	120
	O2	HO2	N3G1	1.88	2.87	174
	O2	HN2G1A	N2G1	2.27	3.12	143
5″	O2	HO2	N7G2	2.24	3.24	172
	N2	HN2	O1A	1.81	2.81	160
6′	N2′	HN2′	O1A	1.99	2.97	174
	N2′	HN2′	O2A	1.96	2.91	163
6″	N2	HN2	O1A	1.99	2.91	151
8′	N2	HN2	O1A	2.07	3.06	170
	N2′	HN2′	O2A	1.98	2.97	164
	N3	HN3	O1A	1.99	2.99	173
	N3′	HN3′	O2A	1.97	2.95	166
8″	N2	HN2	O1A	1.96	2.96	151
	N3	HN3	O1A	1.89	2.89	151
	O2′	HO2′	O1B	2.26	3.26	171
9′	N2	HN2	O1A	1.82	2.82	160
	N2′	HN2′	O2A	1.83	2.83	170
	O2	HO2	N7G1	2.21	3.21	169
	O2′	HO2	N7G2	2.20	3.20	172
9″	O2	HO2	N7G1	1.95	2.94	1.69
	N2	HN2	O1A	2.10	3.04	161

[a] Suffixes (′) and (″) refer to the differing binding modes, as listed in Table V.

Table VII. Binding of Compounds **2–9** to a Deoxythymidyl-(5′→3′)-deoxyadenosine (d(TpA)) Fragment as Modeled by Computer Graphics

compd	binding mode	energy, kcal mol^{-1}		no. of hydrogen bonds
		E_{TOT}	E_{E-S}	
2	minor groove	−61.3	−6.7	0
2	major groove	−70.2	−11.7	1
4	minor groove	−67.9	−10.7	0
4	major groove	−87.8	−31.9	3
5	minor groove	−69.5	−8.2	2
5	major groove	−72.7	−12.9	2
6	major groove	−94.3	−26.0	2
6	spear mode	−81.5	−15.9	1
8	major groove	−128.6	−60.5	4
8	spear mode	−116.5	−43.4	3
9	major groove	−106.3	−31.9	4
9	spear mode	−95.1	−27.1	2

Table VIII. Effect of Compounds **2–9** on Flow L1210 Cells in Culture

drug	dose level for 50% inhibition of L1210 cell growth, μM	
	24 h	48 h
2	8.0	8.0
3	8.0	8.0
4	16.0	16.0
5	8.0	8.0
6	0.6	0.6
7	0.6	0.6
8	1.0	1.5
9	0.6	0.6
mitoxantrone	0.1	0.1

span values of 29–39% were found (Table X), with compound **8** showing the highest values. Intermittent dosing schedules abolished activity. Mitoxantrone showed highly significant activity in this test system, with 30–100% of the treated mice surviving as tumor-free animals. No tumor-free survivors were recorded for the compounds under study. Compounds **6–9** showed statistically significant activity against implanted S180 tumors, with mean percentage reductions in tumor weight of 31–61% being recorded; mitoxantrone showed high levels of activity, although no tumor-free survivors were recorded.

Discussion

The use of computerized molecular modeling in this study has provided reductions of differences in DNA-intercalative behavior between the eight amidoanthraquinones **2–9** examined in this work. The methodology was able to semiquantitate the differences in both energetics and conformations for differing side chains. The possession of four basic nitrogen atoms in the two piperazine rings on the side chains of compound **8** imparts the increase in calculated binding energy compared to **6**, **7**, or **9** and is likely to be a more dominant factor than the greater number of potential hydrogen bonds that **9** can form with the DNA model. It is nonetheless important to bear in mind that the neglect of solvent factors in this study necessarily leads to calculated energies that can only approximate the true ones. The modeling has neglected both the solvent environments that surround these drug–dinucleoside complexes[34,35] and the disruption of bound solvent necessary to produce a complex. The modeling of bound water by, for example, Monte Carlo methods[35] is computationally very expensive and not practicable at present for drug-design studies such as the present one. Molecular mechanics calculations, even neglecting solvent, have consistently been found to be reliable predictors of the geometry of drug–DNA complexes, as in a recent comparative study of actinomycin with oligonucleotide sequences,[36] which found good correspondance with the results of a two-dimensional NMR analysis; conformation

(34) Neidle, S.; Berman, H. M.; Shieh, H. S. *Nature (London)* **1980**, *288*, 129.
(35) Mezei, M.; Beveridge, D. L.; Berman, H. M.; Goodfellow, J. M.; Finney, J. L.; Neidle, S. *J. Biomol. Struct. Dyn.* **1983**, *1*, 287.
(36) Lybrand, T. P.; Brown, S. C.; Creighton, S.; Shafter, R. H.; Kollman, P. A. *J. Mol. Biol.* **1986**, *191*, 495.
(37) Balaji, V. N.; Dixon, J. S.; Smith, D. H.; Venkataraghaven, R.; Murdock, K. C. *Ann. N. Y. Acad. Sci.* **1985**, *439*, 140.
(38) Waring, M. J. *J. Mol. Biol.* **1970**, *54*, 247.

Table IX. Effects on L1210 Leukemia in Vivo

compound	dose, mg/kg	cumulative dose, mg/kg	toxic deaths	mean	% ILS[a]	TFS[b]
saline			0	9.4		0/10
mitoxantrone	0.75		0	16.7	78	7/10
2	25	225	0	9.2	0	0/10
3	25	225	0	9.3	+5	0/10
4	25	225	0	10.0	+13	0/10
5	25	225		9.1	−1	0/10
6	25	225	1	10.8	15	0/10
7	25	225	0	11.7	24	0/10
8	25	225	0	12.3	31	0/10
9	25	225	1	10.3	10	0/10

[a] % ILS = percentage increase in lifespan. [b] TFS = tumor-free survivors.

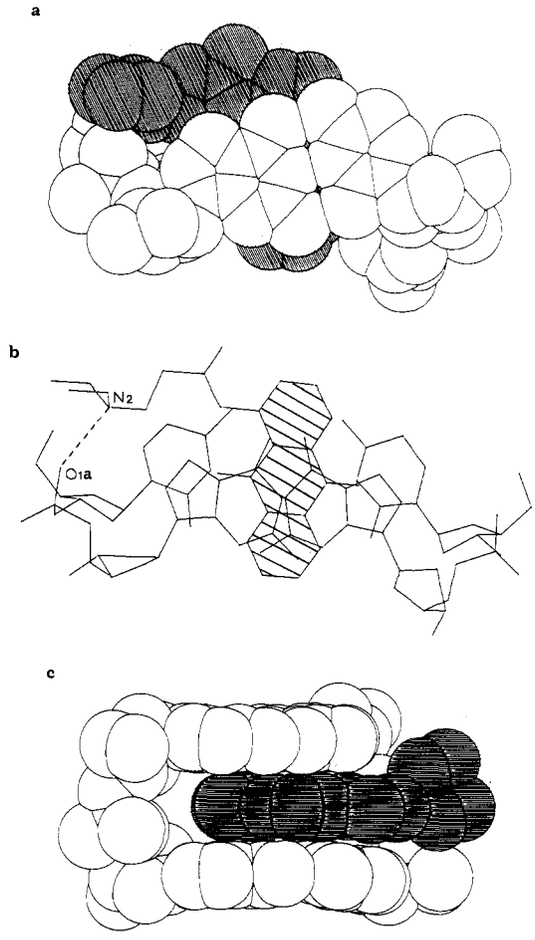

Figure 2. Three computer-drawn views of the low-energy major groove arrangement of compound **2** interacted with a d(CpG) dinucleoside duplex. (a) View looking down onto the least squares of the base pairs; all atoms have been drawn with their van der Waals radii, and the atoms of the drug molecule have been shaded. (b) Skeletal representation of the same view, with the dashed line showing an intermolecular hydrogen bond. The anthraquinone chromophore of **2** has been shaded. (c) Van der Waals representation viewed approximately perpendicular to that in (a), with the drug molecule again being shaded.

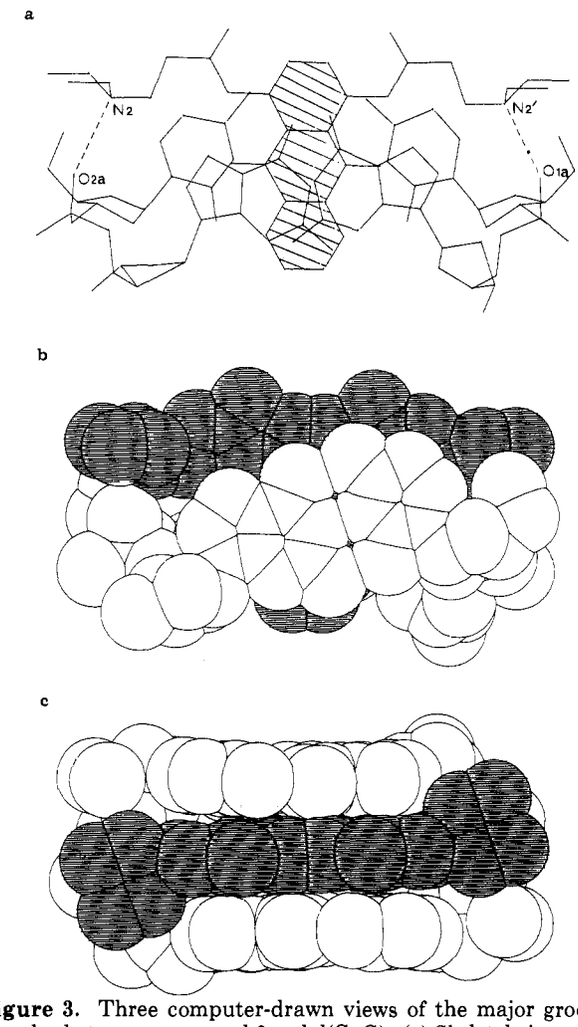

Figure 3. Three computer-drawn views of the major groove complex between compound **6** and d(CpG). (a) Skeletal view onto the plane of the base pairs, with hydrogen bonds drawn as dashed lines. (b) and (c) Van der Waals views, with (c) looking into the major groove.

is largely dependent on nonbonded interactions for which our previous studies have indicated reliable parameterizations.[12,31] There are thus good grounds for the supposition that the *geometries* found here by modeling are meaningful.

The models presented here indicate that the amide groups, even though they are coplanar with the anthraquinone chromophores, do not take part in intercalative stacking interactions with bases, and thus the primary role of the amides is to diminish the flexibility of the side chain compared to their amide analogues.[12] Even though mitoxantrone and related compounds have only a two-carbon chain separating the nitrogen atoms immediately attached to the anthraquinone ring and the basic side-chain nitrogen, this short chain has unconstrained conformational flexibility. This allows the terminal atoms of the chain to form favorable generalized short-range dispersion interactions with the bases, especially with the base nitrogen and electrostatic oxygen atoms that are in the plane of the bases.[12,37] Such arrangements cannot be achieved with the present amidoanthraquinones on account of their less flexible side chains; however, they are of just sufficient length and flexibility in terms of carbon chain between amide groups and basic nitrogen atoms, so that optimal electrostatic interactions can take place with phosphate groups (Figures 3 and 4). These interactions could be at least as significant as hydrogen bonds, although solvent

Table X. Effect of Dosing Schedules of Compounds **5–8** on L1210 Leukemia in Vivo

compound	dose, mg/kg	cumulative dose, mg/kg	schedule[c]	range	mean	% ILS	TFS[b]
saline			A	8–9	8.4		0/10
mitoxantrone	0.4	6.8	B	15–20	17.3	105	7/10
mitoxantrone	3	9	C				10/10
6	50	150	C	6–12	8.4	0	0/10
7	50	150	C	6–10	7.9	−6	0/10
8	50	1.50	C	9–12	10.5	24	0/10
9	50	150	C	6–12	8.6	2	0/10
6	12.5	225	B	10–13	10.9	29	0/10
7	12.5	225	B	9–12	10.6	26	0/10
8	12.5	225	B	10–16	11.7	39	0/10
9	12.5	225	B	8–12	10.6	26	0/10

[a] % ILS = percentage increase in lifespan. [b] TFS = tumor-free survivors. [c] Schedule A, ip days 1–9 (once daily); B, ip days 1–9 (twice daily); C, ip days 1,5, and 9 (once daily).

Table XI. Effects on S180 Tumors in Vivo[a]

compound	dose, mg/kg	cumulative dose, mg/kg	toxic deaths	mean % RTW[b]	% TFS[c]	statistical significance of mean % RTW at the 0.05 level
saline			0		0	NS
2	25	525	0	19	0	NS
2	12.5	263	0	20	0	NS
3	25	525	0	13	0	NS
3	12.5	263	0	10	0	NS
4	25	525	0	21	0	NS
4	12.5	263	0	17	0	NS
5	25	525	0	12	0	NS
5	12.5	263	0	21	0	NS
6	3	63	0	49	0	*SIG
6	6	126	0	42	0	*SIG
6	12	263	0	42	0	*SIG
7	3	63	0	56	0	*SIG
7	6	126	0	45	0	*SIG
7	12	263	0	53	0	*SIG
8	3	63	0	56	0	*SIG
8	6	126	0	29	0	NS
8	12	263	0	46	0	*SIG
9	3	63	0	39	0	*SIG
9	6	126	0	31	0	**SIG
9	12	263	0	61	0	*SIG
mitoxantrone	0.75	16	0	73	0	*SIG

[a] Schedule: days 1–21, ip (once daily). NS = not significant. **SIG = approaching significance. *SIG = significant. [b] Percentage reduction in tumor weight. [c] Percentage of tumor-free survivors.

and counter ions would considerably affect their strength; compounds **6–9** do indeed increase the T_m of DNA to a significantly greater extent than does mitoxantrone, which on the basis of our previous modeling can only have its side chains form hydrogen bonds with DNA. It is also apparent that changes in the nature and dimensions of the $(CH_2)_2$ linkage between amide and basic groups in the present compounds would be deleterious to formation of these electrostatic interactions. The predictions of major groove binding for the side chains of the disubstituted compounds **6–9** on purely steric grounds is in accord with results from both NMR[13] and kinetic[15] studies on the disubstituted anthraquinone mitoxantrone (**1**).

The experiments on the interactions of compounds **2–9** with DNAs in solution have demonstrated that all bind to DNA. The observations of unwinding induced in covalently closed circular DNA show definitively that all of the compounds **2–9** bind intercalatively to DNA[38] and by implication that groove binding in the manner of, for example, netropsin is not their mode of interaction. The compounds are not differentiated one from another on the basis of measured unwinding angles, whereas the equilibrium constants (which are in the usual range for intercalating agents), indicate that the monosubstituted amidoanthraquinones **2–5** interact significantly less strongly than their disubstituted counterparts. This trend is also apparent in the T_m values, with in addition a large preference for the alternating poly[d(AT)]·poly[d(AT)] over the homopolymer poly[d(A)]·poly[d(T)] being shown for all the compounds. Marked differences in binding behavior for these polynucleotides have been noted for other intercalators[39] and is probably due to the adoption of a nonclassical secondary structure for poly[d(A)]·poly[d(T)], as indicated by fiber diffraction[40] and computer modeling,[41] which is unable to accommodate an intercalating molecule with the same facility as B-form DNAs.

The in vivo and in vitro activities of compounds **2–9** follow the trends discussed above, in that there is a marked divergence of behavior for the monosubstituted compared to the disubstituted compounds. The former ones showed little or no activity in the tumor models employed, whereas the latter showed marginal to moderate activity. All compounds were moderately toxic to the growth of L1210 cells in culture, although much less than mitoxantrone. The pattern of toxicities shown in Table VIII is reflected in the activities of these compounds against tumor burdens, which are much lower than for mitoxantrone. However, the clearance rate of **2–9** in animals appears to be much higher than that of mitoxantrone, as judged by the appearance of highly colored (though formally un-

(39) Wilson, W. D.; Wang, Y.-H.; Krishnamoorthy, C. R.; Smith, J. C. *Biochemistry* **1985**, *24*, 3991.
(40) Arnott, S.; Chandrasekaran, R.; Hall, I. H.; Puigjaner, L. C. *Nucleic Acids Res.* **1983**, *11*, 4141.
(41) Rao, S. N.; Kollman, P. *J. Am. Chem. Soc.* **1985**, *107*, 1611.

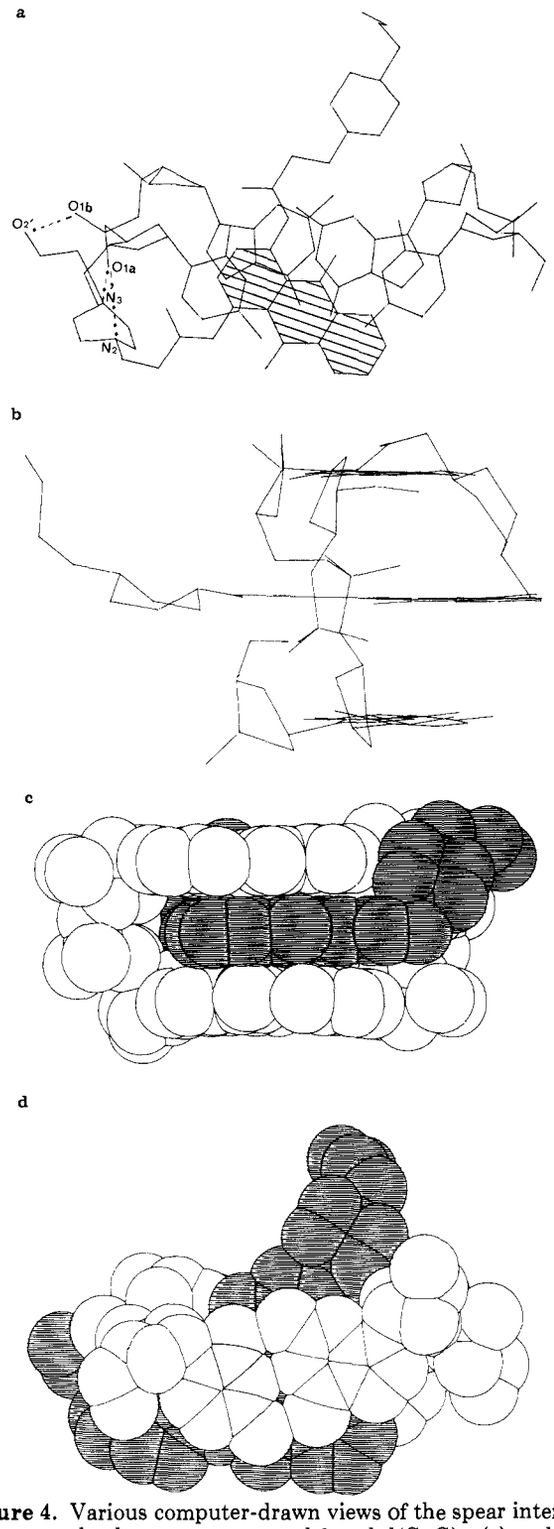

Figure 4. Various computer-drawn views of the spear intercalation complex between compound **8** and d(CpG). (a) and (b) Skeletal views, with (a) projected onto the plane of the base pairs. Hydrogen bonds are shown as dashed lines. The view in (b) is along the vector from the phosphate group of one dinucleotide strand, to that in the other strand. The van der Waals representations in (c) and (d) show the complex at two orthogonal views. In both, the drug molecule is shaded; (c), along the planes of the base pairs and drug molecule chromophore, also shows the steric bulk of the hydroxypiperidine groups of **8**.

identified) anthraquinone metabolites in the urine of the dosed animals within hours of intraperitoneal administration. This would result in lack of systemic cumulative toxicity for the compounds. When they were administered in high doses (24 mg kg^{-1}) over a 21-day period, no toxic effects were observed even though a single dose LD50 of 100 mg kg^{-1} was found for the 1,4-disubstituted compounds. This behavior is in marked contrast to the lengthy persistent behavior of mitroxantrone in dosed animals (D. Collier, unpublished observations). The amidoanthraquinones as a class are probably less metabolically stable than aminoanthraquinones as a result of the lability of the amide linkage.

Thus, the low level of activity of compounds **2–9** may be a result of inherently lower cytotoxicity, for reasons not directly connected with their DNA-intercalative properties, as well as faster metabolism and excretion from animals. The multidisciplinary study reported here has shown that although the possession of DNA-intercalative properties is by itself insufficient to result in antitumor activity, the details of DNA interaction and their relative strengths within a series of compounds do indeed provide qualitative correlations with cytotoxicity and experimental antitumor activity. It is notable that compound **8** is consistently indicated to be the most avid DNA binder in the series, both experimentally and theoretically, and is probably the most active in vivo, at least with the range of conditions and dosing schedules employed.

The relative success here of computer modeling methods, given the necessarily approximate way that they were used, does suggest that they have a useful role in the future development of new antitumor agents that are presumed to be DNA intercalative. Undoubtedly the most effective roles of the techniques will be in the rational design of further analogues of compounds that already show moderate or good activity, as well as the design of radically new intercalators.

Experimental Section

Syntheses. NMR spectra were run on a JEOL FX 100 machine at 100 MHz. UV/visible spectra were recorded on a Pye Unicam SP8-200 machine. Mass spectra were run with a Varian Mat 311A mass spectrometer fitted with an M scan fast atom bombardment source. All spectra were performed by the spectroscopy department at Glaxo Group Research, Greenford, Middlesex, U.K. The hydrochloride salts of **2–9** decomposed at temperatures > 250 °C.

3-(Diethylamino)-*N*-(9,10-dihydro-9,10-dioxoanthracen-1-yl)propanamide Hydrochloride (2). *N*-(9,10-Dihydro-9,10-dioxo-1-anthracenyl)-1-chloropropanamide (**10**) (16.7 mmol, 5 g) was suspended in 1 L of ethanol by vigorous stirring and warmed to 70 °C. Diethylamine (5 mL) in 100 mL of ethanol was added dropwise to the solution over a 1-h period. After a further 6 h, the solvent was removed under reduced pressure to give a yellow solid (4.8 g). This was suspended in water, and 1.1 equiv of dilute aqueous hydrochloric acid was added. The resulting clear yellow solution was filtered and freeze-dried to give a yellow powder, yield (12.9 mmol, 5.0 g) 77%: NMR (D_2O) τ 1.82 (1 H, aromatic, H3), 1.82 (1 H, aromatic, H3), 2.24–2.74 (6 H, aromatic), 6.43 (2 H, CH_2N), 6.60 (4 H, NCH_2CH_3), 7.07 (2 H, $COCH_2$), 8.56 (6 H, CH_3); IR (cm^{-1}) 3100–3660 (NH), 2200–2750 (N^+H), 1705 (amide), 1660–1640 (quinone), 1592, 1580, 710 (aromatic); UV/vis (cm^{-1}) (H_2O) λ_{max} 263, E_1^1 848; λ_{max} 396, E_1^1 108; MS, m/z 351, 224 (weak). Anal. Calcd for $C_{21}H_{22}N_2O_3HCl\cdot 2H_2O$: C, 59.64; H, 6.64; N, 6.62; Cl, 8.38. Found: C, 59.38; H, 5.78; N, 6.51; Cl, 8.5.

***N*-(9,10-Dihydro-9,10-dioxo-1-anthracenyl)-1-piperidinepropanamide Hydrochloride (3).** *N*-(9,10-Dihydro-9,10-dioxoanthracen-1-yl)-1-chloropropanamide (**10**) (16.7 mmol, 5 g) was suspended in ethanol by vigorous stirring and warmed to 70 °C. Piperidine (5 mL) was added dropwise over a half-hour period, and the mixture then was incubated for a further 6 h. The solvent was removed under reduced pressure to give a yellow solid (5 g). This was suspended in water, and 1.1 equiv of dilute aqueous hydrochloric acid was added. The resulting clear yellow solution was filtered and freeze-dried to give a yellow powder, yield (4.96 g, 12.2 mmol): NMR (D_2O) τ 1.80–2.04 (1 H, aromatic; H2, 7.74, 8.60 (6 H, aliphatic); IR (cm^{-1}) 2180–2760 (NH), 3040–3650 (NH^+), 1710 (amide), 1665–1640 (quinone), 1590–1580 (aromatic); UV/vis

(cm^{-1}) (H_2O) λ_{max} 263, E_1^1 886, λ_{max} 397, E_1^1 110; MS, m/z 362. Anal. Calcd for $C_{22}H_{22}N_2O_3HCl·0.5H_2O$: C, 65.05; H, 5.76; N, 6.79; Cl, 8.69. Found: C, 64.78; H, 5.93; N, 6.87; Cl, 8.69.

***N*-(9,10-Dihydro-9,10-dioxo-1-anthracenyl)-3-[4-(3-hydroxypropyl)piperazin-1-yl]propanamide Hydrochloride (4).** *N*-(9,10-Dihydro-9,10-dioxo-1-anthracenyl)-3-chloropropanamide (**10**) (18.4 mmol, 5.5 g) was suspended in 1 L of ethanol by vigorous stirring. The mixture was heated to 70 °C, and 8 g of 1-piperazinepropanol in 100 mL of ethanol was added dropwise. The mixture was incubated for 4 h, and the solvent was removed under reduced pressure to give a yellow solid. This was recrystallized from toluene/ethanol, giving 5 g of yellow crystals. A 4.5-g portion of this product was then dissolved in ethanol, and 2 equiv of dilute aqueous hydrochloric acid was added. The solvent was removed under reduced pressure to leave a yellow powder, yield (4.67 g, 9.5 mmol) 52%: NMR (D_2O) τ 1.71 (1 H, aromatic, H2), 2.2–2.48 (4 H, aromatic, H5–8), 2.48–2.64 (2 H, aromatic, H2, H4), 6.00–6.64 (14 H, aliphatic), 6.98 (2 H, aliphatic, $NHCOCH_2$), 7.90 (2 H, aliphatic, $CH_2CH_2CH_2$); IR (cm^{-1}) 2000–2750 (NH), 3040–3640 (NH, OH), 1690 (amide), 1665, 1635 (quinone), 1590, 1578, 715 (aromatic); UV/vis (cm^{-1}) (H_2O) λ_{max} 263, E_1^1 668, λ_{max} 397.5, E_1^1 85; MS, m/z 422. Anal. Calcd for $C_{24}H_{27}N_3O_4HCl·1.25H_2O$: C, 56.75; H, 6.05; N, 8.27; Cl, 12.7. Found: C, 56.69; H, 5.74; N, 8.26; Cl, 12.

***N*-(9,10-Dihydro-9,10-dioxo-1-anthracenyl)-2-(2-hydroxyethyl)-1-piperidinepropanamide Hydrochloride (5).** *N*-(9,10-Dihydro-9,10-dioxoanthracenyl)-3-chloropropanamide (**10**) (13.4 mmol, 4 g) was suspended in 1 L of ethanol by vigorous stirring. The mixture was heated to 60 °C, and 6 g of 1-piperidineethanol in 100 mL of ethanol was added dropwise. The mixture was incubated for 16 h, and the solvent was removed under reduced pressure. The resulting material was washed thoroughly with water and then cold ethanol to give 4.04 g of a yellow solid. This was suspended in distilled water, and 1 equiv (11.4 mM) of hydrogen chloride as an aqueous solution was added. The clear yellow solution produced was stirred for 30 min, filtered, and freeze-dried to a yellow powder, yield (3.95 g, 9.9 mmol) 74%: NMR (D_2O) τ 1.95 (1 H, aromatic, H2), 2.30–3.00 (6 H, aromatic, H3–H8), 5.98–7.32 (9 H, aliphatic), 7.60–8.56 (8 H, aliphatic); IR (cm^{-1}) 2000–2780 (NH), 3050–3660 (NH, OH), 1700 (amide carbonyl), 1672, 1640 (quinone carbonyl); UV/vis (cm^{-1}) (H_2O) λ_{max} 262, E_1^1 747; λ_{max} 395, E_1^1 96; MS, m/z 406. Anal. Calcd for $C_{24}H_{26}N_2O_4·1.2HCl·1.5H_2O$: C, 60.40; H, 6.38; N, 5.87; Cl, 8.92. Found: C, 60.65; H, 5.87; N, 6.01; Cl, 8.8.

***N*,*N*′-(9,10-Dihydro-9,10-dioxo-1,4-anthracenediyl)bis[3-(diethylamino)propanamide] Dihydrochloride (6).** *N*,*N*′-(9,10-Dihydro-9,10-dioxo-1,4-anthracenediyl)bis(3-chloropropanamide) (**11**) (11.5 mmol, 5 g) was suspended in 1 L of ethanol with stirring. The mixture was warmed to 60 °C, and 4 mL of diethylamine was added dropwise over a 1-h period. After 18 h, the solvent was removed under reduced pressure to yield a brown solid. After recrystallization from ethanol/toluene, 4 g of brown crystals remained. These were suspended in ethanol, and 2 equiv (16.3 mM) of aqueous hydrogen chloride was added. The solvent was stirred for 30 min and filtered. The resulting brown solution was freeze-dried to a brown powder, yield (6.9 mmol, 3.95 g) 60%: NMR (D_2O) τ 1.66 (2 H, aromatic, H2,3), 2.24 (2 H, aromatic, H5,8), 2.36 (2 H, aromatic, H6,7), 6.64 (4 H, aliphatic, CH_2CH_2N), 6.63 (8 H, aliphatic, CH_3CH_2N), 7.02 (4 H, aliphatic, $NHCOCH_2$), 8.58 (12 H, aliphatic, NCH_2CH_3); IR (cm^{-1}) 2100–2740 (NH), 3160, 3380 (NH), 1700 (amide carbonyl), 1640 (quinone carbonyl), 598, 1580, 735 (aromatic); UV/vis (cm^{-1}) (H_2O) λ_{max} 255, E_1^1 693; λ_{max} 447, E_1^1 86; MS, m/z 492. Anal. Calcd for $C_{28}H_{24}N_4O_4·2HCl·1H_2O$: C, 57.63; H, 6.91; N, 9.93; Cl, 12.2. Found: C, 57.32; H, 6.70; N, 9.64; Cl, 12.4.

***N*,*N*′-(9,10-Dihydro-9,10-dioxo-1,4-anthracenediyl)bis(1-piperidinepropanamide) Dihydrochloride (7).** *N*,*N*′-(9,10-Dihydro-9,10-dioxo-1,4-anthracenediyl)bis(3-chloropropanamide) (**11**) (3.2 mmol, 1 g) was suspended in 500 mL of ethanol with stirring. The mixture was warmed to 60 °C, and 3 mL of piperidine was added dropwise as a solution in ethanol over a 1-h period. After incubation at 60 °C for 18 h, the solution was cooled and filtered, and the solvent was removed under vacuum. After the product was washed with water and dried, 1.08 g of a brown crystalline solid remained. After the product was washed with water and dried, 1.08 g of a brown crystalline solid remained. A 500-mg (0.9-mmol) portion of this was suspended in water, and 2 equiv of dilute aqueous hydrochloric acid was added. The resulting clear brown solution was filtered and freeze-dried to give a brown powder, yield 0.84 mmol (465 mg): ^1H NMR (D_2O) τ 1.57 (1 H, aromatic, H2), 2.0–2.36 (4 H, aromatic, H5,8), 6.12–6.60 (8 H, CH_2N), 6.60, 7.20 (8 H, $COCH_2CH_2N$), 7.72–8.60 (12 H, piperidine ring); IR (cm^{-1}) 220–3670 (NH, NH, water), 1710 (amide), 1630 (quinone), 1592, 1585 (aromatic), 1508 (amide II); UV/vis (cm^{-1}) (H_2O) λ_{max} 256.5, E_1^1 627; λ_{max} 445.5, E_1^1 86; MS, m/z 516. Anal. Calcd for $C_{30}H_{42}N_4O_4·2HCl·4H_2O$: C, 53.97; H, 7.85; N, 8.39; Cl, 10.62. Found: C, 54.66; H, 6.19; N, 8.36; Cl, 10.6.

***N*,*N*′-(9,10-Dihydro-9,10-dioxo-1,4-anthracenediyl)bis[4-(3-hydroxypropyl)-1-piperazinepropanamide] Tetrahydrochloride (8).** *N*,*N*′-(9,10-Dihydro-9,10-dioxoanthracenediyl)-bis(3-chloropropanamide) (**11**) (10.3 mmol, 4.3 g) was suspended in 1.5 L of ethanol with stirring. The mixture was warmed to 70 °C, and 5 g of piperazine-1-propanol was added, as a solution in ethanol, over a 1-h period. After 4 h, a futher 3 g of amine was added as an ethanolic solution, and the mixture was reincubated for a further 18 h. The resulting clear brown solution was then filtered, and the solvent was removed under vacuum to leave a brown powder (4.5 g). This was suspended in 500 mL of water, and 4 equiv of dilute aqueous hydrochloric acid was added. The mixture was stirred for 40 min, filtered, and freeze-dried to give a brown powder, yield (6.6 mmol, 5.15 g) 64%: ^1H NMR (D_2O) τ 1.30–1.42 (2 H, aromatic, H2,3), τ 1.90–2.10 (4 H, aromatic, H5–8), τ 6.92 (32 H, aliphatic), τ 7.72–8.06 (4 H, aliphatic, $CH_2CH_2CH_2$); IR (cm^{-1}) 2500–3600 (OH, NH, ^+NH); UV/vis (cm^{-1}) (H_2O) λ_{max} 255.5, E_1^1 462; λ_{max} 447, E_1^1 87; MS, m/z 634. Anal. Calcd for $C_{34}H_{46}N_6O_6·4HCl·6.5H_2O$: C, 45.49; H, 7.07; N, 9.36; Cl, 15.80. Found: C, 45.97; H, 6.13; N, 9.37; Cl, 16.0.

***N*,*N*′-(9,10-Dihydro-9,10-dioxo-1,4-anthracenediyl)bis[2-(2-hydroxyethyl)-1-piperidinepropanamide] Dihydrochloride (9).** *N*,*N*′-(9,10-Dihydro-9,10-dioxo-1,4-anthracenediyl)bis(3-chloropropanamide) (**11**) (1.2 mmol, 0.5 g) was suspended in 1 L of ethanol with stirring. The mixture was warmed to 70 °C, and 5 mL of 2-piperidineethanol was added dropwise as an ethanolic solution over a 1-h period. After 16 h, the solvent was removed under reduced pressure to give a sticky solid. This was washed thoroughly with water to give 0.6 g of a brown solid. A 0.5-g portion of this was suspended in distilled water, and 2 equiv of dilute aqueous hydrochloric acid was added. The solution was stirred for 10 min, filtered, and freeze-dried to give a brown powder, yield (460 mg, 0.71 mmol) 46%: NMR (D_2O) τ 1.38–1.52 (2 H, aromatic, H3,4), 2.00–2.18 (4 H, aromatic, H5–8), 5.92–720 (26 H, aliphatic), 7.40–8.0 (16 H, aliphatic); UV/vis (cm^{-1}) (H_2O) λ_{max} 255, E_1^1 597; λ_{max} 447.5, E_1^1 73; IR (cm^{-1}) 1700 (amide), 1640 (quinone), 2200–3600 (NH, OH, NH); MS, m/z 605. Anal. Calcd for $C_{34}H_{44}N_4O_6·2HCl·2.5H_2O$: C, 56.50; H, 6.76; N, 7.75; Cl, 9.81. Found: C, 56.25; H, 6.66; N, 7.52; Cl, 10.1.

***N*-(9,10-Dihydro-9,10-dioxo-1-anthracenyl)-1-chloropropanamide (10).** 1-Aminoanthraquinone (13 mmol, 3 g) was dissolved in 1 L of toluene containing a catalytic amount of pyridine. The mixture was warmed to 60 °C, and 6 mL of 3-chloropropionyl chloride was added dropwise over a 1-h period. After the mixture was stirred for 4 h, the solvent was removed under reduced pressure to give a yellow solid. The product was washed with water and recrystallized from cold toluene/ethanol, yield (3.14 g, 10 mmol) 77%: ^1H NMR ($CDCl_3$) τ −2.43 (1 H, br, NH), 0.93 (1 H, aromatic, H2), 1.66–1.91 (2 H, aromatic, H5,8), 1.98 (1 H, aromatic, H4), 2.10–2.42 (3 H, aromatic, H3,6,7), 6.06 (2 H, CH_2Cl), 6.98 (2 H, $COCH_2$); IR (cm^{-1}) 3080–3360 (NH), 1690 (amide), 1672, 1645 (quinone), 1595, 1597 (aromatic), 1520 (amide II); MS, m/z 313; mp 176 °C. Anal. Calcd for $C_{17}H_{12}NO_3Cl$: C, 65.03; H, 3.36; N, 4.46; Cl, 11.13. Found: C, 65.36; H, 3.84; N, 4.33; Cl, 10.7.

***N*,*N*′-(9,10-Dihydro-9,10-dioxo-1,4-anthracenediyl)bis(1-chloropropanamide) (11).** 1,4-Diaminoanthracene-9,10-dione (12.8 mmol, 3 g) was suspended in 1 L of toluene containing a catalytic amount of pyridine. The mixture was warmed to 70 °C, and 5 mL of 3-chloropropionyl chloride was added dropwise over a 1-h period. After being stirred for 4 h, the mixture was cooled, and the solvent was removed under reduced pressure to give a red-brown crystalline solid. This was washed thoroughly with ethanol to give the pure product, yield (2.92 g, 6.7 mmol) 52%: ^1H NMR ($CDCl_3$) τ −2.67 (2 H, br, NH), 0.88 (2 H, aromatic, H2,3),

1.77 (2 H, aromatic, H5,8), 2.21 (2 H, aromatic, H6,7), 6.07 (4H, CH_2Cl), 7.00 (4 H, $NHCOCH_2$); IR (cm^{-1}) 3000–3310 (NH), 1705, 1695 (amide), 1640 (quinone), 1595, 1585 (aromatic), 1510 (amide); MS, m/z 419, mp 189 °C.

X-ray Crystallography. The amidoanthraquinone **4** was recrystallized from dichloromethane as orange-red elongated primatic needles. Preliminary X-ray data were obtained by Weissenberg and oscillation photography. Accurate cell dimensions were obtained by means of least-squares refinement of 25 θ values, measured on an Enraf-Nonius CAD4 diffractometer with Ni-filtered Cu Kα radiation. Cell dimensions were a = 15.803 (2) Å, b = 7.034 (1) Å, c = 21.018 (2) Å, β = 110.55 (1)°, and the space group was assigned as $P2/a$. Intensity data was collected in the range 1.5° < θ < 65°, with an ω–2θ scan technique and a maximum scan time of 100 s/reflection. A periodic check on the intensities of three control reflections showed no crystal decay. A total of 4213 independent reflections were collected, of which 2240 had $I > 3\sigma(I)$ and were used in the subsequent refinement. The crystal structure was solved by direct methods and refined by full-matrix least-squares techniques. Some hydrogen atom positions were located from difference Fourier synthesis; others were calculated from standard geometric considerations. All hydrogen atom parameters were kept fixed during the refinement, which converged to a final R of 0.051 and R_w of 0.044 with weights $w = 1/\sigma^2[R_o + 0.03F^2]$. Final non-hydrogen atom fractional coordinates are given in Table IV.

Energy and Computer Graphics Calculations. The molecular energy of a particular intercalation complex between an amidoanthraquinone **2–9** and a dinucleoside phosphate duplex model for intercalated DNA was approximated as

$$E_{TOT} = E_{N\text{-}B} + E_{TORS} + E_{E\text{-}S}$$

The nonbonded parameterizations used in the $E_{N\text{-}B}$ term have been described in detail elsewhere. Partial charges on the protonated forms of the drug molecules were calculated by CNDO/2 methods.[42] Those for the dinucleosides were taken from ref 43. A distance-dependent dielectric constant was used in the electrostatic component such that $\epsilon = 1$ for $r_{ij} < 3$ Å, $\epsilon = 0.75r_{ij} - 1.25$ for 3 Å < r_{ij} < 7 Å, and $\epsilon = 4$ for $r_{ij} > 7$ Å. Torsional barrier heights were taken from ref 44 and 45. The molecular structures of compounds **2–3** and **5–9** were generated with the MOLEC5 program by using both standard geometric criteria and the features found in the crystal structures of **4**. This program has been written for the Gresham-Lion Supervisor 214 raster graphics system, which is linked to a VAX 11/750 computer. It enables real-time molecular manipulations (translation, rotation, torsion, and angle changes) to be made on a molecule or arrangements of molecules. Interactive docking of **2–9** into low-energy positions in the intercalation cavities of the dinucleosides dCpG and dTpA was performed with the MOLEC5 molecular graphics program,[46] which calculated the energies E_{TOT} and also interactively monitored distances between potential hydrogen-bond donors and acceptors and included hydrogen bonds implicitly in the energy calculations. Tables V and VI detail the major low-energy forms found for the complex. Lists of coordinates for these are obtainable from S. Neidle.

DNA Binding in Solution. Calf thymus DNA was purchased from the Sigma Chemical Co. as the type 1 highly polymerized sodium salt. Closed circular duplex DNA (pAT153 and pBR322 DNAs) were prepared by the alkali lysis method of Manniatis after Birnboim and Doty. Synthetic oligomers were purchased from Sigma. SHE buffer (2 mM HEPES, 10 M EDTA, and 9.4 mM NaCl, pH 6.8μ = 0.01) and MES buffer (2 mM MES, 10 M EDTA, and 0.5 M NH_2F, pH 6.4μ = 0.5) were also used. DNAs were dissolved in the appropriate buffer by extensive dialysis. Particulate material was removed by spinning at 10 000 rpm for 10 min in an MSE ultracentrifuge. Calf thymus DNA was sonicated to approximately 4 × 10^5 daltons (molecular weight determined by gel electrophoresis). Extinction coefficients used in the determination of the concentration of DNA solutions are shown in Table II.

Determination of Equilibrium Binding Constants. Binding curves were measured by spectrophotometric methods with a Cary 219 UV/vis spectrophotometer. All drugs obey Beer's law over the range of concentrations used, and all spectral curves of the drug, when titrated with DNA, pass through a common, isosbestic point if the drug concentration is kept constant.

Titration of drug solutions with DNA at low ionic strength (μ = 0.01) resulted in rapid precipitation of a highly colored, fibrous, drug–DNA complex. At high ionic (μ = 0.5) strength, drug–DNA interactions are sufficiently weakened to avoid this effect, and so NH_2–MES buffer has been used throughout.

For determination of free and bound drug concentrations, 3 mL of a drug solution (between 0.2 and 0.08 mM) was placed in a 3-mL quartz cuvette. Aliquots of 10–50 μL of calf thymus DNA were then added, and after careful mixing the absorbance, the visible maximum of the drug was recorded. Absorbance was then normalized for the dilution effect, and titration was continued until the normalized absorbance remained constant (usually at a phosphated/drug ratio of less than 30). Values of r (binding ratio) and C (free drug concentration) were then calculated by the method of Skerrett and Peacocke. These were fed directly into an algorithm designed to calculate best-fit parameters of $K(0)$ (equilibrium binding constant for an isolated potential binding site) and n (number of sites occluded by one bound drug species) by satisfying the modified Scatchard equation of McGhee and Von Hippel.

Nucleic Acid Melting. Melting curves were recorded with a Gilford spectrophotometer fitted with a heated cell holder. All spectra were plotted directly onto a Southern Instruments plotter. All nucleic acids used were dissolved in SHE buffer (μ = 0.01). For all runs, 330-μL, 1-cm quartz cuvettes were used. For calf thymus DNA, 300 μL of a solution containing 0.1 mM DNA and 0.01 mM appropriate drug was used. For synthetic polymers, 300 μL of a solution containing 0.05 mM DNA and 0.005 mM drug was used. Solutions were heated at 1 °C/min over the temperature range 25–95 °C, and the absorbance change was monitored at the appropriate wavelength. For the calculation of the transition melting (T_m) value, the mid point of the absorbance change was taken and used to read off the appropriate value on the temperature scale.

Determination of Unwinding Angles. All viscometric measurements were performed using a Poulten, Seife, and Lee (Wickfor, Essex) U tube viscometer, Model BS/1P/MSL type 1, with a constant C value of 0.002 965 mm^2. pBR3322 (2.5 mL) or the closely related but slightly smaller pAT153 closed-circular supercoiled DNA, at an accurately known concentration of approximately 0.2 mM, was placed in the viscometer. The flow time of the DNA solution was then measured in triplicate by using a hand-held digital stopwatch, such that the maximum spread of time between separate readings was less than 0.07% of total flow time for each run. The DNA was then titrated with drug at 200–400 μM in aliquots between 5 and 20 μL, delivered by a calibrated 25-μL Gilson pipet fitted with a polythene extension tube previously soaked in drug solution to minimize absorption effects. Drug solutions were mixed in by carefully passing air through the reservoir mixture.

Plots of drug:DNA ratio nucleotides were then constructed to determine the V_{app} at the principal maximum of the titration. For one drug (**3**), a plot of C_T against N_T at the principal maximum was constructed to ensure that a linear relationship existed. V_{app} for each titration was found to be equivalent to that calculated by graphical means.

For each batch of plasmid, V_{app} was calculated first for ethidium bromide, and then the unwinding angle ϕ_D was calculated for the test drug relative to this figure, assuming the unwinding angle for ethidium bromide to be 26° by means of the relationship

$$\phi_D/\phi_E = V'_D/V'_E = V_{app}$$

where ϕ_D and ϕ_E are the unwinding angles for the drug and ethidium, and V'_D and V'_E are their equivalent binding ratios required for relaxation of the supercoiled DNA.

(42) Hudson, B. D.; Neidle, S. *Int. J. Biol. Macromol.* **1987**, *9*, 193.
(43) Nakata, V.; Hopfinger, A. J. *FEBS Lett.* **1980**, *117*, 259.
(44) Islam, S. A.; Neidle, S. *Acta Crystallogr., Sect. B: Struct. Sci.* **1983**, *B39*, 114.
(45) Hopfinger, A. J. *Conformational Properties of Macromolecules*; Academic: New York, 1973.
(46) Islam, S. A. Ph.D. Thesis, University of London, 1986.

Growth Inhibition of Tumor Cells in Vitro and in Vivo L1210 Cells in Culture. Medium A consisted of RPMI 1640 with 25 mM HEPES plus 10% fetal calf serum and 10% DMSO. Medium B consisted of RPMI 1640 with 25 mM HEPES plus 10% fetal calf serum, 25 mM L-glutamine, 200 units/mL of benzylpenicillin, and 200 μg/mL of streptomycin.

L1210 cells were obtained from Flow Laboratories Ltd. A 48-h culture flask initially seeded at 10^5 cells/mL was aspirated gently and a 1:50 dilution in isotonic saline made from a 1-mL sample. Cells were counted with a Coulter counter (Coulter Electronics Ltd).

The stock was then diluted to 2×10^5 cells/mL in medium B and incubated for a further 24 h at 37 °C, giving an exponentially growing culture. Cells were counted as before, and the stock was diluted to 10 cells/mL in medium B. Plastic petri dishes were then seeded with 3 mL of the cell suspension at 10^5 cells/mL.

Drug solutions were made in phosphate-buffered saline such that when 50 μL of this solution was added to 3 mL of the cell suspension the appropriate final concentration was achieved. Initially, drug concentrations over a wide range, such as 100, 25, and 1 μM, were made up in order to localize the effective range of the drug. Once this was known, a range of levels around the concentration needed to give 50% inhibition of cell growth relative to the control were set up. The control cells were dosed with 50 μL of phosphate-buffered saline. A positive control (mitoxantrone) was also set up. Each dose level was set up in triplicate. The cells were incubated at 37 °C in a humidified atmosphere containing 5% carbon dioxide and counted after 24 and 48 h with a Coulter counter.

Intraperitoneally Implanted L1210 Tumor. The tumor was stored at 10^6 cells/mL in liquid nitrogen as a suspension in medium A. The cells were diluted in medium B for passage, which was performed weakly in DBA/2 female mice by transfer of cells growing intraperitoneally; 2×10^5 cells per mouse is inoculated. For experimental chemotherapy, BD2F mice were used.

Tumors were prepared for experimental chemotherapy by removing intraperitoneal fluid from a passage mouse into 10 mL of medium B. Cells were counted with an improved Neubauer hasmocytometer, and the stock solution was correspondingly diluted to give 2.5×10^5 cells/mL. Next, 0.2 mL of this solution was implanted intraperitoneally in BD2F female mice, giving a final inoculum of 5×10^4 cells/mouse.

Innoculated animals were divided into groups of 10, one group per treatment. Control groups were set up by using the drug diluent, one being employed for each dosing schedule within the experiment. A positive control, using the known active standard compound mitoxantrone, was also set up. All dosing was ip against the ip tumor.

Subcutaneously Implanted S180 Tumors. The tumors are stored at 10^6 cells/mL in liquid nitrogen as a single cell suspension in medium A. Passage was performed fortnightly in female CRH mice by transfer of cells growing subcutaneously in the right lower inguinal region; 0.2 mL of a suspension containing 10^6 cells/mL were used, giving a total inoculum of 2×10^5 cells/mouse. CRH female mice were also used for experimental chemotherapy.

Tumor suspensions were prepared by killing 8–10 mice containing a tumor that had been implanted 14 days previously. The tumors were placed in medium B containing 1% DNase to prevent coagulation of cells by released DNA. The tumors were minced with fine scissors, and the cells were ground to a single cell suspension with a tissue grinder. A count of viable cells was made with a hemocytometer, and the suspension was diluted to 10^6 cells/mL.

Experimental animals were prepared in the same manner as passage mice. On day 0 (day of inoculation), animals were randomly divided into groups of 10, weighed, and earmarked. A negative control group was set up, with the drug diluent as dosage. A positive control, using a known active standard mitoxantrone, was also set up.

Animals were dosed ip against the subcutaneous tumor. They were individually weighed at intervals of about 3 days starting from day 4. Tumor size was measured with electronic calipers for recording the width and length of the tumor. Measurements commenced on day 9, and measurements were recorded every 3–4 days until the tumors reached 4 g in weight.

Compounds were considered to have activity if tumor weight over a group was reduced by 35% or greater relative to the controls.

Acknowledgment. This work was supported by Glaxo Group Research Limited and the Cancer Research Campaign. D.A.C. thanks Glaxo Limited and the Science and Engineering Research Council for a CASE studentship. We are grateful to Drs. C. Spillings and M. Elves (Glaxo) for continuing support and encouragement and their staff for help in the biological testings reported here. Drs. S. Islam and R. Kuroda are thanked for their assistance in X-ray crystallography and molecular modeling, and Dr. Z. H. L. Abraham is thanked for help and advice on drug–DNA binding and for supplying the computer program used for analysis of binding plots.

Registry No. **2**, 112764-13-3; **2** (free base), 112764-21-3; **3**, 112764-14-4; **3** (free base), 112764-22-4; **4**, 112764-15-5; **4** (free base), 112764-23-5; **5**, 112764-16-6; **5** (free base), 112764-24-6; **6**, 112764-17-7; **6** (free base), 112764-25-7; **7**, 112764-18-8; **7** (free base), 112764-26-8; **8**, 112764-19-9; **8** (free base), 112764-27-9; **9**, 112764-20-2; **9** (free base), 112764-28-0; **10**, 20210-30-4; diethylamine, 109-89-7; piperidine, 110-89-4; 1-piperazinepropanol, 5317-32-8; 1-piperidineethanol, 3040-44-6; 1-aminoanthraquinone, 82-45-1; 3-chloropropionyl chloride, 625-36-5; 1,4-diaminoanthracene-9,10-dione, 128-95-0.